SANDIA REPORT

SAND2001-3417
Unlimited Release
Printed November 2001

Molecular Self-Assembly

John G. Curro, John D. McCoy, Amalie L. Frischknecht, and Kui Yu

Prepared by
Sandia National Laboratories
Albuquerque, New Mexico 87185 and Livermore, California 94550

Sandia is a multiprogram laboratory operated by Sandia Corporation, a Lockheed Martin Company, for the United States Department of Energy under Contract DE-AC04-94AL85000.

Sandia National Laboratories

Issued by Sandia National Laboratories, operated for the United States Department of Energy by Sandia Corporation.

Available to DOE and DOE contractors from
U.S. Department of Energy
Office of Scientific and Technical Information
P.O. Box 62
Oak Ridge, TN 37831

Telephone: (865)576-8401
Facsimile: (865)576-5728
E-Mail: reports@adonis.osti.gov
Online ordering: http://www.doe.gov/bridge

Available to the public from
U.S. Department of Commerce
National Technical Information Service
5285 Port Royal Rd
Springfield, VA 22161

Telephone: (800)553-6847
Facsimile: (703)605-6900
E-Mail: orders@ntis.fedworld.gov
Online order: http://www.ntis.gov/ordering.htm

SAND 2001 – 3417
Unlimited Release
Printed November 2001

Molecular Self-Assembly

LDRD Project: 32573

Final Report

John G. Curro
Materials & Process Modeling & Computation Dept.
Sandia National Laboratories
P. O. Box 5800
Albuquerque, New Mexico 87185-1349

John D. McCoy
Department of Materials & Metallurgical Engineering
New Mexico Institute of Mining & Technology
Socorro, New Mexico 87801

Amalie L. Frischknecht
Materials & Process Modeling & Computation Dept.
Sandia National Laboratories
P. O. Box 5800
Albuquerque, New Mexico 87185-1349

Kui Yu
Materials Chemistry Dept.
Sandia National Laboratories
P. O. Box 5800
Albuquerque, New Mexico 87185-1349

Abstract follows

Abstract

This report is divided into two parts: a study of the glass transition in confined geometries, and formation mechanisms of block copolymer mesophases by solvent evaporation-induced self-assembly.

The effect of geometrical confinement on the glass transition of polymers is a very important consideration for applications of polymers in nanotechnology applications. We hypothesize that the shift of the glass transition temperature of polymers in confined geometries can be attributed to the inhomogeneous density profile of the liquid. Accordingly, we assume that the glass temperature in the inhomogeneous state can be approximated by the T_g of a corresponding homogeneous, bulk polymer, but at a density equal to the average density of the inhomogeneous system. Simple models based on this hypothesis give results that are in remarkable agreement with experimental measurements of the glass transition of confined liquids.

Evaporation-induced self-assembly (EISA) of block copolymers is a versatile process for producing novel, nanostructured materials and is the focus of much of the experimental work at Sandia in the Brinker group. In the EISA process, as the solvent preferentially evaporates from a cast film, two possible scenarios can occur: microphase separation or micellization of the block copolymers in solution. In the present investigation, we established the conditions that dictate which scenario takes place. Our approach makes use of scaling arguments to determine whether the overlap concentration c* occurs before or after the critical micelle concentration (CMC). These theoretical arguments are used to interpret recent experimental results of Yu and collaborators on EISA experiments on Silica/PS-PEO systems.

Part 1 – The Glass Transition in Confined Geometries

As the trend of using polymers in microelectronic and other applications involving smaller features continues, it is important to recognize that the physical properties of polymers in confined geometries are not necessarily the same as for the corresponding bulk polymers. Perhaps the most important physical property that characterizes a polymer material is the glass transition temperature. For these reasons the effect of confining geometries on the glass transition temperature has been a topic of considerable recent interest in the polymer community. In this investigation we suggest a possible mechanism that accounts for these effects [1]. Experiments show very rich, nonuniversal behavior. In some cases very large shifts (>50°C) of T_g in thin films [2,3] and in pores [4] are observed. While the glass temperature is typically lower in the confined geometry, experiments also indicate cases where T_g increases as well [5,6]. Recent theories for the effect of confinement on T_g by deGennes [7] and Long and Lequeux [8] employed free volume and percolation concepts.

We propose that the essential cause of the shift in the glass transition of a liquid in a confined geometry is that its density under confinement is inhomogeneous. Although difficult to measure, x-ray reflectivity experiments [9] and simulations [10] have demonstrated that layering over a few molecular diameters exists near the surface in thin liquid films. When an experiment is performed to measure the glass transition temperature of a liquid under these conditions, what is measured is an average response of the entire liquid within the confined space. Our model simply assumes that density can be pre-averaged. In other words, we hypothesize that the glass transition of the inhomogeneous, confined fluid would be approximately the same as for a bulk liquid having the same density as the average density of the confined liquid. Variations of this

hypothesis have been suggested by Long and Lequeux [8] and Reiter [11] as a contributing factor to the change in T_g in thin films. In this paper we implement this idea through simple models and find that it is able to explain many of the experimental observations regarding changes in T_g in confined geometries. The attractiveness of this approach is that it begs the question of what molecular mechanisms are responsible for the glass transition. No detailed theory for the dynamics of liquids is needed.

For discussion purposes, we consider a liquid in a slit geometry. In Fig. 1.1 we schematically illustrate the process of introducing two impenetrable surfaces into a uniform bulk liquid of particles having a diameter σ. (For the case of polymer liquids we identify σ with the statistical segment length.) As a consequence of introducing the surfaces, the particles that are shaded must be removed when the impenetrability constraint is turned on. Hence in the slit geometry, the environment that a molecule sees is different near the surface than in the bulk liquid resulting in a nonuniform density profile. If the particles in the channel are in equilibrium with the bulk fluid, the density distribution will adjust itself to enforce equality of chemical potentials of the liquid within the slit and in bulk.

First consider the average density within a channel of width H. In the bulk liquid depicted on the left in Fig. 1.1, the average density ρ_{slit} can be written as the number of particles N whose centers are within the channel divided by the volume $\rho_{slit} = N / A H$, where A is the cross sectional area of the channel. Since in the bulk liquid, the particle centers are distributed randomly within the slit, the average density is, of course, equal to the bulk density ρ_{bulk}. By contrast, when the impenetrability constraints are turned on, the centers of the particles can no longer exist in the region within $\sigma/2$ of the walls as seen by the dotted lines in the right hand side of Fig. 1.1. We can express the average density for the confined system as

$$\rho_{slit} = \frac{N}{AH} = \rho_{bulk} + \frac{2\Gamma(H)}{H} \tag{1.1}$$

where $\rho(z)$ is the density profile within the slit and $\Gamma(H)$ is the surface excess defined according to $\Gamma(H) = 0.5\int_0^H [\rho(z) - \rho_{bulk}]dz$. The density profile, and hence ρ_{slit}, can be computed using standard methods.

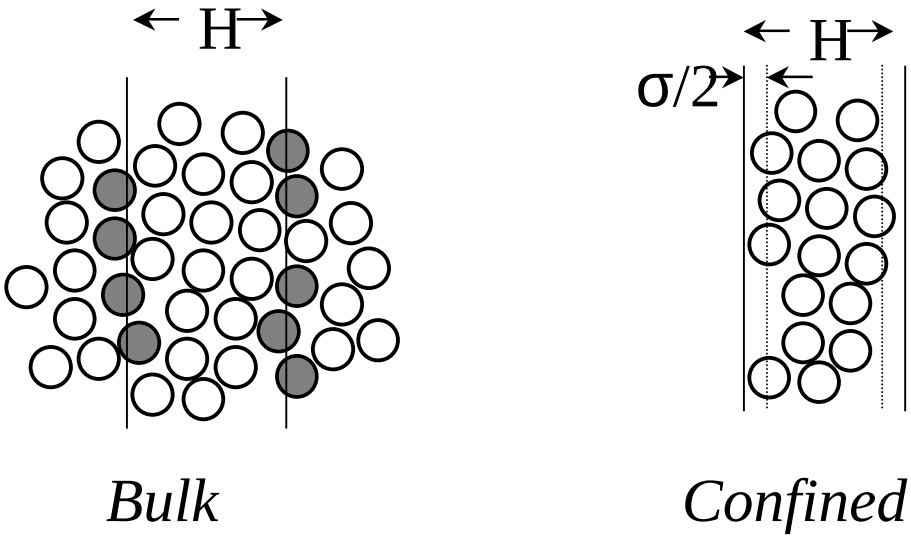

Figure 1.1 Schematic of a liquid confined to a slit

Based on our hypothesis, we approximate the shift in the glass transition temperature from the bulk value $\Delta T_g = T_g - T_g^{\infty}$ as

$$\Delta T_g = \left(\frac{dT_g}{dP}\right)\left(\frac{\partial P}{\partial \rho}\right)_T (\rho_{slit} - \rho_{bulk}) \tag{1.2}$$

which is valid for small ΔT_g. Eq. (1.2) can be expressed in a form that can be used for predictive purposes

$$\Delta T_g = \frac{1}{\kappa_T}\left(\frac{dT_g}{dP}\right)\frac{2\Gamma(H)}{H\rho_{bulk}} \qquad (1.3)$$

where κ_T is the isothermal compressibility obtainable from PVT measurements of the bulk liquid. The pressure derivative of the glass transition has been measured experimentally on a number of glass forming liquids [12]. Hence the shift in the glass transition due to confinement can be estimated from experimental data on bulk liquids if we are able to compute or measure the surface excess.

For a bulk liquid the surface excess is defined to be zero. When the impenetrability of the surfaces is enforced, the surface excess becomes a nonuniversal function that depends on the polymer architecture and the balance between polymer/polymer and polymer/surface attractive interactions. For illustrative purposes, we will first introduce what we term as the *primitive model* which incorporates the known, qualitative features of the density profile near a wall. In this model we take the density $\rho(z)$ to be: 0 for $0 \le z < \sigma/2$; ρ^* for $\sigma/2 \le z < \xi + \sigma/2$; and ρ_{bulk} for $\sigma/2 + \xi \le z \le H/2$ where ρ^* is the average density in the first layer of width ξ. This length ξ plays the role of a correlation distance over which a monomer feels the presence of the wall. For this simplified profile we find from Eq. (1.3) a convenient expression for the shift in the glass transition

$$\Delta T_g = \frac{-1}{\kappa_T}\left(\frac{dT_g}{dP}\right)\frac{\sigma}{H}\left[1 - \frac{2\xi}{\sigma}\left(\frac{\rho^*}{\rho_{bulk}} - 1\right)\right] \qquad (1.4)$$

Under most conditions, where there is a balance between monomer/monomer and wall/monomer attractions, $\rho^* \sim \rho_{bulk}$ and we expect the T_g of the polymer in the slit to be lower than the bulk

glass transition temperature. However, if the wall/monomer attractions are very high then $\rho_{bulk} < \rho^* < 1.22\sigma^{-3}$ and we see from Eq. (1.3) that the T_g of the confined polymer can be greater than its bulk value. The upper limit on ρ^* is constrained by the random closed packed density which would result in jamming of the monomers near the wall. We also observe from Eq. (1.3) that ΔT_g is linearly related to the reciprocal of the slit width. These predictions seem to be in qualitative accordance with many experiments on liquids in confined geometries [4].

The primitive model is only a qualitative approximation for the actual density profile in a confined geometry. A more quantitative approach that we follow here is classical Density Functional Theory (DFT) [13]. DFT can be viewed as an alternative to a full, many-chain simulation in which a self-consistent field approximation is made to enhance the efficiency of the calculation. In particular, the full interactions between molecules and the wall are retained, while the correlations between molecules are included through a self-consistent field $\psi[\rho(z)]$ that we approximate as

$$\psi[\rho(z)] = 1 - \sqrt{1 + 2\int C_0(r - r')\Delta\rho(z')d\vec{r}} - \frac{1}{kT}\int v_a(r - r')\Delta\rho(z')d\vec{r} \qquad (1.5)$$

where $C_0(r)$ is the direct correlation function of a hard core reference system and $v_a(r)$ is the attractive part of the potential between intermolecular sites. This field may be thought of as an additional interaction between the wall and the polymer repeat units whose purpose is to mimic the effect on the density profile due to intermolecular correlations between macromolecules. The inverse problem of calculating the density profile $\rho[\psi(z)]$ can be solved numerically for the freely jointed chain model used here. More complex polymer models require the inverse problem

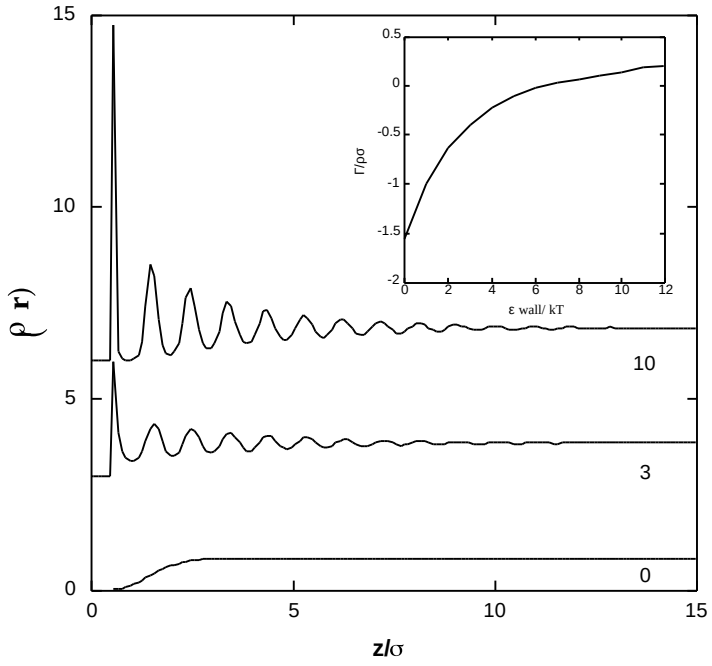

Figure 1.2 - The density profile vs. distance from the wall for wall-well depths of 0, 3, and 10 in units of kT. The profiles are offset for clarity. In the inset, the surface excess is shown for varying wall strengths. In all cases, the bulk density was 0.85 σ^3; the chain length was 20; and the depth of the site-site square well potential was 1.142 kT.

to be carried out through a single chain computer simulation. The interested reader is referred to reference [13] for details of the method.

In this investigation the polymer attractions $v_a(r)$ were modeled as a square well potential of depth ε and width $\sigma/2$. The surface attractions $v_w(r)$ were taken to have a cubic dependence on the distance z from the wall as would be expected at large distances from a van der Waals surface. Density profiles for this model are plotted in Fig. 1.2 for various strengths of the wall attractions corresponding to: (1) a non-wetting wall, (2) comparable wall and chain interactions, and (3) a strongly attractive wall. In these calculations, the slit width was taken to be infinite. With zero wall attraction, the contact density against a hard wall is simply related to the pressure $\rho(z = \sigma/2) = P/kT$. As the strength of the square well attractions increases from zero, the

pressure of the bulk liquid, and the contact density both decrease. In this manner, ε was adjusted to give P~1 atm. for sites 1 nm in diameter and density 0.85 nm^{-3}. Conversely, increasing the wall attractions at fixed intermolecular interactions can be seen to increase the contact density and structure in the density profiles. In the inset we show the surface excess computed for infinite channel spacing. Not surprisingly, for large channels we find that Γ is independent of H and that $\Delta T_g \quad \sigma/H$. For small slit spacings, however, we find a more complex dependence of ΔT_g on H.

It can be seen from Fig. 1.2 that the surface excess increases as the wall attractions increase until, at wall attraction of about 7 kT, it becomes positive. In view of Eq. (1.3), we would predict that ΔT_g would also change from negative to positive at this point. Thus for most cases where the wall attractions are weak or comparable to the intermolecular interactions, our hypothesis predicts that the T_g of the confined polymer would be less than the bulk value. Only for strong wall interactions would the glass transition temperature of the confined polymer be larger than the corresponding bulk T_g. These findings are in qualitative accordance with the primitive model, experimental observations, and computer simulations [14].

It is difficult to make detailed quantitative comparisons between theory and experiment because of the nonuniversal nature of the phenomenon and the relative simplicity of the models we employed. Nevertheless we will attempt to see if our simple hypothesis and models lead to the correct order of magnitude of experimental observations. For illustrative purposes let us consider polystyrene (PS) for which experiments [12] give $dT_g/dP = 0.031\text{K/atm}$, $\kappa_T = 3.877\text{x}10^{-5}\text{atm}^{-1}$ and $\kappa_T^{-1}\left(dT_g/dP\right) = 801\text{K}$. From this data we can see that the T_g shift is very sensitive to the average slit density. As a measure of the magnitude of the

confinement effect on T_g we have chosen to focus on the "T_g increment" defined as the derivative $d\Delta T_g/d(1/H)$. In Table 1 we summarize our predictions for this derivative from various models. The calculations were done for PS assuming that the statistical segment length σ was 1nm. Reasonable parameters for the primitive model were chosen: neutral wall ($\rho^* = \rho_{bulk}$), strongly attractive wall ($\rho_{bulk}\sigma^3 = 0.85,\ \rho^*\sigma^3 = 1.22,\ \xi = 1.5\sigma$), and non-wetting wall ($\rho^* = 0,\ \xi = 1.5\sigma$). The DFT calculations in Table 1.1 used the same parameters as in Fig. 1.2.

Table 1.1 - Simple Model calculations for PS

Model	**Wall**	**$d\Delta T_g/d(1/H)$**
Primitive	non-wetting	-3204,
	neutral	-801
	strong	+245
HS N=1	hard	-200
HS N=20	hard	-232
Sq. Well	non-wetting	-2500
	neutral	-620
	strong	+229

To illustrate the general trends that are seen in the literature, the T_g increment was extracted from selected experimental data and is tabulated in Table 1.2. First consider the case of liquids in small pores. In order for such experiments to be possible it is obviously necessary for the liquid to wet the surface of the pores, suggesting neutral to strongly attractive surfaces. The primitive model results in Table 1.1 for the neutral surface (-801Knm) and strongly attractive wall (+245Knm) can be seen to bracket the experimental results on pores for a range of liquids and surfaces. A better estimate is provided by the DFT results in Table 1 for hard (ε_{wall}=0), neutral ($\varepsilon_{wall}/kT = 3$), and strongly attractive ($\varepsilon_{wall}/kT = 10$) walls. Furthermore, we see from Table 1.1 that there is very little difference in the DFT predictions for monomers(N=1) and chains (N=20). This

demonstrates that the shift in glass temperature in a pore geometry is essentially independent of molecular weight in accordance with experiment.

Let us now turn our attention to the data on unsupported films in Table 1.2. It can be observed that the T_g increment is much larger for films than for the case of liquids in pores. The calculations performed in the present investigation were designed for the case of polymers near walls, whereas the unsupported films correspond to an air/polymer interface. Nevertheless, one can argue that qualitatively, the air/polymer interface would correspond approximately to a polymer against a non-wetting surface as seen in Fig. 1.2. This can be mimicked in the primitive model by taking $\rho^* = 0$. As seen in Table 1, this leads to an estimate of –3204Knm for the T_g increment in rough agreement with typical experimental results in Table 1.2. DFT calculations for a non-wetting wall give –2500Knm, also the right order of magnitude for unsupported films.

Table 1.2 – Selected data on T_g in confined geometries

Liquid	**dΔTg/d(1/H)**	**MW**
SiOx Pores*		
0-terphenyl [4]	-60 to -135	
Benzyl alcohol [4]	-20 to -30	
Propylene glycol [5]	+45	
Polypropylene glycol [5]	-2 to +16	400 to 4K
Unsuported Films		
Polystyrene[2,3]	-1400 to -4700	116 to 9100K

* SiO_x Surfaces are "treated" in various manners to control their hydrophobic nature. T_g increment in units of Knm.

A striking feature of the data in Table 1.2 on unsupported films is the strong increase in the T_g increment as the molecular weight increases. This is in sharp contrast to what is observed in pore geometries where there is virtually no molecular weight effect. Examination of Eq. (1.4)

reveals that a possible source of a molecular weight dependence for unsupported films is through the correlation length ξ. For neutral and strongly attractive walls we expect [15] that ξ would correspond roughly to the mesh size in a polymer melt and be independent of molecular weight. For an air/polymer interface, however, the density is very low near the surface and it is reasonable to associate ξ with the radius of gyration. This argument leads to a glass transition temperature shift that increases as N^{ν} where ν is the Flory exponent. Experiments [2,7] suggest a somewhat stronger molecular weight dependence for unsupported films. A more careful analysis based on DFT calculations of the air/polymer interface, rather than a wall geometry, is required in order to make a more detailed comparison with experiments on unsupported films.

In this paper we proposed a simple, yet plausible hypothesis that maps an anisotropic, confined liquid to a corresponding isotropic, bulk liquid at the average of the anisotropic density. Using a simple primitive model, as well as DFT to compute the average density of monatomic and chain molecule confined liquids, we are able to predict many of the trends seen in experimental measurements of T_g in small pores and films. In particular we find: 1) ΔT_g is usually negative but changes to positive for strongly attractive surfaces.; 2) ΔT_g is linear in 1/H for large channel spacings.; 3) ΔT_g is much more dramatic and always negative for free standing films; 4) ΔT_g is independent of molecular weight in pores. Remarkably, the predictions from our simple hypothesis give the correct order of magnitudes for shifts in the glass temperatures. We emphasize that the approach we have taken has avoided any detailed considerations regarding the dynamics of the molecules in anisotropic, confined geometries. Surely these details will be important for describing other properties. Finally we emphasize that more quantitative

comparisons of ΔT_g could be made in the future by employing more detailed models of the polymer and surfaces, and the air/polymer interface.

Part 2 – Formation Mechanisms of Block Copolymers in the EISA Process

Since the discovery of surfactant-templated silica mesophases [16] a number of formation mechanisms have been proposed[16-19]. Generally, it is acknowledged that the presence of surfactants in a solution guides the formation of the silica/surfactant mesostructures [16-21].

Very recently, Kui et al. reported the preparation of mesostructured silica films with large characteristic length scales through solvent evaporation-induced self-assembly (EISA), using polystyrene-*block*-poly(ethylene oxide) (PS-*b*-PEO) diblock copolymers as structure-directing agents [22-24]. Due to PS hydrophobicity, the diblocks used, such as PS(215)-*b*-PEO(100) which has 215 styrene units and 100 ethylene oxide units, do not mix with either water or ethanol. Water and ethanol are the two solvents that are traditionally used in the preparation of mesostructured silica when small molecular weight surfactants, such as poly(ethylene oxide)-*b*-poly(propylene oxide)-*b*-poly(ethylene oxide) (PEO-*b*-PPO-*b*-PEO), are used as structure-directing agents [23,24]. Thus, a different synthesis method was employed [22-24].

This novel preparation method began with a dilute homogeneous solution of a silica precursor (tetraethoxysilane, TEOS) and a diblock copolymer in a mixture of tetrahydrofuran (THF) and water. After this dilute solution was cast, THF preferentially evaporated, which caused a solvent quality decrease for the PS block as well as a concentration increase of the species in the depositing film. At some critical point, cooperative self-assembly of both the PS-*b*-PEO diblock and the silicate started, which led to the formation of liquid-crystalline

mesophases.

Kui et al. observed the trapping of intermediates in the mesophase transition from lamellae to normal hexagonally arranged cylinders and/or to normal spheres with a cubic array distributed in a hydrophilic matrix. This work will be described in detail elsewhere [25]. One important aspect of this work is our fundamental understanding of the formation process of the silica/diblock mesophases. No micellization is likely involved in the mesophase formation of the present system, which begins with a dilute homogeneous solution; we argue that the copolymer chains reach their overlap concentration (c^*) before the critical micellization concentration (CMC), during the process of THF preferential evaporation. Below we describe our calculations leading to this conclusion.

It should be pointed out that nonaqueous cosolvents influence the kinetics of TEOS hydrolysis as well as subsequent condensation. Therefore, such kinetics becomes very intricate in the course of THF preferential evaporation, which causes changes in the solvent composition and quantity. Due to the cooperative assembly of silicates with the diblock copolymer, this complicated kinetics of silicate chemistry plays a very important role in the formation of liquid-crystalline mesophases. However, this study does not address the problem of the silicate chemistry, which takes place simultaneously with the cooperative self-assembly.

In a typical synthesis, PS(180)-*b*-PEO(120) diblock copolymer was dissolved in tetrahydrofuran (THF) at 2wt.%. Afterwards, a certain amount of tetraethoxysilane (TEOS), hydrogen chloride (HCl), and water (Milli Q) were added to the dilute solution of the copolymer in THF. The quantity of TEOS added was such as to achieve a volume ratio of 40% copolymer to 60% silica, under the assumption that TEOS converts completely to silica. The total amount of HCl and water added was such as to achieve mole ratios of 1TEOS : 0.004HCl : $5H_2O$. After

30 minutes of sonication, one drop of the solution was cast to obtain a diblock/silica film, and the THF was allowed to evaporate.

Thus the synthesis starts with a dilute homogeneous solution with low water content, and the diblock exists in the form of single chains. As THF preferentially evaporates from the cast solution, the species concentration in the film increases and the solvent quality for the PS block decreases. At some critical point, when the concentration of the diblock copolymer and silicates is high enough and the solvent quality is poor enough, a disorder-to-order transition occurs.

During this process of the THF evaporation, the cast solution may go through a micellization transition before the transition to the ordered phase. On the other hand, the cast solution may not experience micellization but may go directly from the disordered (single chain phase) to the ordered phase, since the diblock copolymer single chains may reach the overlap concentration before they reach the critical micellization concentration (CMC). In this case there should be a direct disorder-to-order transition without an intervening micellar phase.

We can estimate the overlap concentration c using the following scaling arguments [15]. Here we neglect the contribution of the silicates and only consider the diblock and the two solvents, water and THF. The polymer coils start to overlap when

$$\frac{4}{3}\pi R_g^3 c \approx 0.7 \qquad (2.1)$$

where R_g is the radius of gyration of the coil, and we have assumed close packing of the coils. For the present system of diblocks, an upper bound on c is the overlap concentration of each block considered separately. In general the radius of gyration of a coil in solution is

$$R_g^2 = \frac{b^2 N^{2\nu}}{6} \qquad (2.2)$$

where b is the statistical segment length, N is the number of segments, and the Flory exponent ν depends on whether the block is in a good, theta, or bad solvent , depending on the value of the Flory χ parameter:

$$\nu = \begin{cases} 3/5 & \chi < 1/2 \\ 1/2 & \chi \approx 1/2 \\ 1/3 & \chi > 1/2 \end{cases} \tag{2.3}$$

The relation between the length and molecular weight of a chain is given by the characteristic ratio [27] :

$$C_\infty = \frac{\langle R^2 \rangle_0 m_0}{Ml^2} \tag{2.4}$$

where M is the molecular weight of the chain, m_0 is the molecular weight of a monomer, l is the bond length, and $\langle R^2 \rangle_0 = 6R_g$ is the mean-square end-to-end distance of the chain. We can use C_∞ to map the statistical segment length b and number of segments N to the monomer bond length l and degree of polymerization N_p by requiring the contour lengths and the radii of gyration in theta conditions to be equal:

$$\begin{aligned} bN &= lN_p \\ b^2N &= C_\infty l^2 N_p \end{aligned} \tag{2.5}$$

so that $b = C_\infty l$ and $N = N_p / C_\infty$. Substituting into Eq. (2.2), we can express the radius of gyration of a chain as

$$R_g = \frac{C_\infty^{1-\nu} l N_p^\nu}{\sqrt{6}} \tag{2.6}$$

so that the overlap concentration due to overlap of a single block is

$$c^* \approx \frac{0.17}{R_g^3} \approx \frac{2.5}{C_\infty^{3-3\nu} l^3 N_p^{3\nu}} \tag{2.7}$$

Here c is the number of blocks (and thus the number of chains) per volume at the overlap threshold. This corresponds to a weight concentration of diblock chains of

$$c_w = c \frac{\left(m_0^{PS} N_p^{PS} + m_0^{PEO} N_p^{PEO}\right)}{N_A} \tag{2.8}$$

where N_A is Avogadro's number. Using R_g for either the PS or PEO block alone, c gives the number overlap concentration, while c_w gives the weight fraction of diblock that corresponds to that number concentration of the single block.

In the present system, both blocks are initially in a good solvent, but as the THF evaporates the solvent quality worsens for the PS. We find that for PS, C_∞=10, m_0 = 104, and l = 2.1 Å in the melt at 413 K.[26,27] We thus find that for the PS block with N_p = 180 the overlap concentration is approximately c_w = 0.059 g/cm^3 in a good solvent, c_w = 0.14 g/cm^3 in a theta solvent, and c_w = 0.6 g/cm^3 in a bad solvent. Similarly for PEO, C_∞ = 4, m_0 = 44, and l = 2.98 Å in the melt at 413 K. For the PEO block with N_p = 120 the overlap concentration is approximately c_w = 0.127 g/cm^3 in a good solvent, which is the case here. An upper bound for c_w is the lowest of these values for a given solvent quality, since the diblock will certainly be overlapped once one of the blocks by itself is overlapped. Thus, the maximum overlap concentration is c_w = 0.059 g/cm^3 in good solvent conditions for the PS (due to overlap of the PS blocks) and c_w = 0.127 g/cm^3 in all other conditions (due to overlap of the PEO blocks).

A lower bound on the overlap concentration can be obtained by assuming that the overall radius of gyration of the diblock in solution is simply the sum of the radii of gyration for the two blocks considered separately. From Eqs (2.7)and(2.8), in this case we have

$$c_w \approx \frac{0.17}{\left(R_g^{PS} + R_g^{PEO}\right)^3} \left(\frac{m_0^{PS} N_p^{PS} + m_0^{PEO} N_p^{PEO}}{N_A} \right) \qquad (2.9)$$

We can crudely take into account the change in solvent quality for the PS block by using a different Flory exponent from Eq. (2.3) in the calculation of R_g^{PS} depending on the value of the Flory χ parameter. We estimate χ from the solubility parameters for PS, THF, and water:

$$\chi = \frac{V_s}{RT} \left(\delta_{PS} - \left(x_w \delta_w + x_{THF} \delta_{THF} \right) \right)^2 \qquad (2.10)$$

Here x_w and x_{THF} are the volume fractions of water and THF, respectively. The solubility parameters are δ_{PS} = 18 MPa$^{1/2}$, δ_w = 47.9 MPa$^{1/2}$, and δ_{THF} = 18.6 MPa$^{1/2}$ [27,28]. We take the molar volume of the solvent to be a weighted sum of the water and THF molar volumes, $V_s = x_w v_w + x_{THF} v_{THF}$. We can thus calculate a lower bound for c_w from Eqs. (2.3), (2.9) and (2.10) as a function of the THF concentration.

The results of our calculations for the overlap concentration are shown in Figure (2.1). The solid line shows the trajectory in the ternary phase diagram that the present system follows as the THF evaporates, assuming that none of the water evaporates and neglecting the small volume contribution from the silicate. The dashed lines show the lower bound and the dotted lines show the upper bound for c_w; the square point shows the CMC for 2% (wt) diblock copolymer in THF as water is added [28]. Figure 2.1 shows that we cannot determine definitively whether the system is always above the overlap concentration without more extensive analysis, but we note that the upper bound is probably a significant overestimate, since it entirely neglects the presence of the second block. Therefore, it is plausible that the system crosses the overlap concentration before the CMC and thus exhibits a direct disorder-to-order transition.

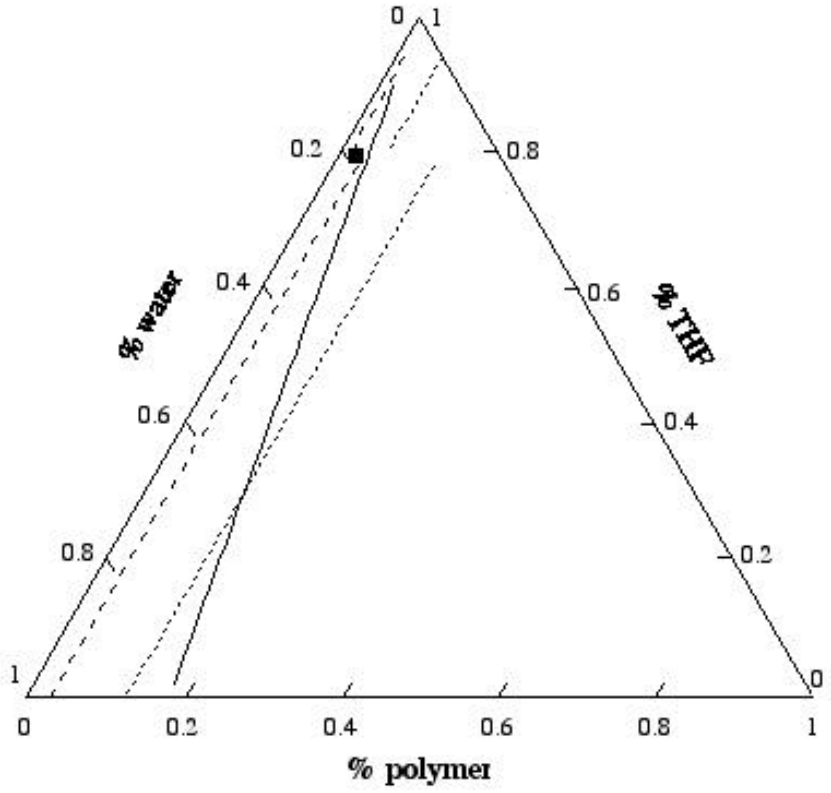

Figure 2.1. Ternary phase diagram for the present system. The solid line is the trajectory of the system as the THF evaporates. The lower (dashed lines) and upper (dash-dot lines) bounds of the copolymer overlap concentration are shown, with the discontinuity occurring as the solvent quality for the PS block changes from good to bad. The square point shows the CMC for a system of 2% (wt) copolymer.

References

1. J. D. McCoy and J. G. Curro, *Phys. Rev. Lett.*, submitted (2001).
2. J. A. Forrest, K. Dalnoki-Veress, J. R. Stevens, and J. R. Dutcher, *Phys. Rev. Lett*. **77**, 2002 (1996). J. A. Forrest and J. Mattsson *Phys Rev. E* **61**, R53 (2000).
3. K. Dalnoki-Veress, J. A. Forrest, C. Murray, C. Gigault, and J. R. Dutcher, *Phys. Rev. E* **63**, 031801 (2001).
4. C. L. Jackson and G. B. McKenna, Chem. Mater. **8**, 2128 (1996); *J. Non-Cryst. Solids* **131-133**, 221 (1991); J.-Y. Park and G.B. McKenna, *Phys. Rev. B* **61**, 6667 (2000).
5. J. Schuller, Y. B. Melnichenko, R. Richert,and E. W. Fisher, *Phys. Rev. Lett.* **73**, 2224 (1994). Y.B. Melnichenko, J. Schuller, R. Richert, B. Ewen and C.-K. Long
   J. Chem. Phys. **103**, 2016 (1995). J. Schuller, R. Richert and E.W. Fischer *Phys. Rev. B* **52**, 15232 (1995).
6. D. S. Fryer, P. F. Nealey, and J. J. dePablo, *Macromolecules* **33**, 6439 (2000).
7. P. G. de Gennes, *Eur. Phys. Journal E* **2**, 201 (2000).
8. D. Long and F. Lequeux, *Eur. Phys. Journal E* **4**, 371 (2001).
9. C. J. Yu, A. G. Richter, A. Datta, M. K. Durbin, and P. Dutta, *Phys Rev. Lett* **82**, 2326 (1999).
10. A. Yethiraj and C. K. Hall, *J. Chem. Phys.* **91**, 4827 (1989).
11. G. Reiter, *Macromolecules* **27**, 3046 (1994).
12. L. H. Sperling, *Introduction to Physical Polymer Science* (Wiley, New York, 1986).
13. J. B. Hooper, J. D. McCoy, and J. G. Curro, *J. Chem. Phys*. **112**, 3090 (2000); J. D. Hooper, M. T. Pileggi, J. D. McCoy, J. G. Curro, and J. D. Weinhold, *J. Chem. Phys.* **112**,

3094 (2000); J. D. Hooper, J. D. McCoy, J. G. Curro, and F. B. van Swol, *J. Chem. Phys.* **113**, 2021 (2000).

14. J. A. Torres, P. F. Nealy, and J. J. de Pablo, *Phys. Rev. Lett*. **85**, 3221 (2000).
15. P. G. de Gennes, *Scaling Concepts in Polymer Physics* (Cornell University Press, Ithaca).
16. C. Kresge, M. Leonowicz, W. Roth, C. Vartuli, J. Beck *Nature* **359** 710 (1992).
17. C. Y. Chen, S. L. Burkett, H. X. Li, M. E. Davis, *Microporous Mater.* **2**, 27 (1993).
18. A. Monnier, F. Schuth, Q. Huo, D. Kumar, D. Margolese, R. S. Maxwell, G. D. Stucky, *Science* **261**, 1299 (1993).
19. J. Y. Ying, C. P. Mehnert, M. S. Wong, *Angew. Chem. Int. Ed.* **38**, 57 (1999).
20. Y. Lu, R. Ganguli, C. Drewien, M. Anderson, C. J. Brinker, W. Gong, Y. Guo, H. Soyez, B. Dunn, M. Huang, J. Zink, *Nature* **389**, 364-368 (1997).
21. C. J. Brinker, Y. Lu, A. Sellinger, H. Fan, *Adv. Mater.* **11**, 579 (1999).
22. K. Yu, C. J. Brinker,A. J. Hurd, A. Eisenberg, "PS-*b*-PEO/Silica Films with Regular and Reverse Mesostructures of Large Characteristic Length Scales Prepared by Solvent Evaporation-Induced Self-Assembly", *Polymer Preprints*, **42***(1)*, 659 (2001).
23. K. Yu, C. J. Brinker, A. J. Hurd, A. Eisenberg, "Formation of PS-*b*-PEO/Silica Films with Flat or Curved Multi-Bilayer Mesostructures of Large Characteristic Length Scales Prepared by Solvent Evaporation-Induced Self-Assembly", *Polymeric Materials: Science & Engineering Preprints* **84**, 796 (2001).
24. (a) K. Yu, C. A. Drewien, A. J. Hurd, C. J. Brinker, A. Eisenberg, A. "Formation Mechanism of Silica/Diblock Mesophases by Solvent Evaporation-Induced Self-Assembly", *Materials Research Society (MRS) Proceedings.* (2001) *accepted*. (b) K. Yu, C. J. Brinker, Unpublished results.

25. K. Yu, A. L. Frischknecht, C. A. Drewien, A. J. Hurd, C. J. Brinker, *Macromolecules* (2001) submitted.

26. L. J. Fetters, D. J. Lohse, D. Richter, T. A. Witten, A. Zirkel, A. *Macromolecules* **27**, 4639 (1994).

27. J. Brandrup, E. H. Immergut, *Polymer Handbook*, 3rd Ed.; Wiley-Interscience: New York, (1989) VII 38, VII526.

28. K. Yu, Ph.D. *thesis* (1998) (Dept. of Chem. McGill Univ.) Chapter 7.

Distribution

1	MS 0188	LDRD Office
1	MS 1411	Eliot Fang
1	MS 1411	Gary S. Grest
1	MS 1411	Mesefin Tsige
1	MS 1349	Frank van Swol
1	MS 1411	B. G. Potter
1	MS 1349	Jeffrey Brinker
1	MS 0316	Laura J. D. Frink
1	MS 0316	Mark J. Stevens
1	MS 0316	Aidan P. Thompson
10	MS 1349	John G. Curro
10	MS 1349	Amalie L. Frischknecht

1	MS 9018	Central Technical Files, 8945-1
2	MS 0899	Technical Library, 9616
1	MS 0612	Review & Approval Desk, 9612
		For DOE/OSTI